

Embodied Intelligence for Advanced Bioinspired Microrobotics: Examples and Insights

Néstor O. Pérez-Arancibia

Abstract—The term *embodied intelligence* (EI) conveys the notion that body morphology, material properties, interaction with the environment, and control strategies can be purposefully integrated into the process of robotic design to generate intelligent behavior; in particular, locomotion and navigation. In this paper, we discuss EI as a design principle for advanced microrobotics, with a particular focus on co-design—the simultaneous and interdependent development of physical structure and behavioral function. To illustrate the contrast between EI-inspired systems and traditional architectures that decouple sensing, computation, and actuation, we present and discuss a collection of robots developed by the author and his team at the *Autonomous Microrobotic Systems Laboratory* (AMSL). These robots exhibit intelligent behavior that emerges from their structural dynamics and the physical interaction between their components and with the environment. Platforms such as the Bee⁺⁺, RoBeetle, SMALLBug, SMARTI, WaterStrider, VLEIBot⁺, and FRISSHBot exemplify how feedback loops, decision logics, sensing mechanisms, and smart actuation strategies can be embedded into the physical properties of the robotic system itself. Along these lines, we contend that co-design is not only a method for empirical optimization under constraints, but also an enabler of EI, offering a scalable and robust alternative to classical control for robotics at the mm-to-cm-scale.

I. INTRODUCTION

Traditionally, in the fields of robotics and modern control, sensing, perception, decision-making, and actuation are treated as distinct modules implemented and connected through electronics for communication, signal processing, and control. This architecture—ubiquitous from industrial manipulators to autonomous vehicles—relies heavily on centralized programmable controllers and logics. In contrast, the concept of *embodied intelligence* (EI) is based on the notion that complex behavior can emerge from the physical interaction between a robot's structural components, its materials, and its environment. According to this analytical framework, morphology and materials are not merely physical properties of a robot's body, but active elements in the processes of sensing, actuation, computation, and control. Automated motion patterns and feedback for functionality, stability, and, foreseeably, for decision-making can be *encoded* in the structure and dynamics of the physical system itself.

The basic principles underlying EI—namely, the integration of sensing, actuation, computation, and control into the physical structure of a system—can be conceptually traced back to ancient mechanical devices. One of the earliest known examples is Ktesibios' clepsydra (water clock), which used float-regulated valves to maintain a constant water level, thus embodying feedback control through direct material interaction with the environment [1]. Similar principles can be identified in the automata developed by Hero of Alexandria, who is believed to have designed steam-driven and air-powered devices capable of performing complex

sequences of actions through intelligent use of mechanical linkages and timing mechanisms [2]. During the so-called Islamic Golden Age, Al-Jazari built programmable automata and water clocks that incorporated float valves, cams, and timing mechanisms—advancing the integration of structure and behavior [3].

More recently, in the early 19th century, J. M. Jacquard introduced a system of punch cards to control weaving patterns, which represents an early fusion of mechanical structure with encoded behavior [4]. Perhaps, the most well-known system exhibiting some key features of EI—such as electronics-free control—is J. Watt's centrifugal governor, which additionally is considered to be the most direct antecedent to modern feedback control systems. This mechanism was widely used in Victorian England to regulate the speeds of steam engines via a purely mechanical feedback loop that tightly coupled actuation and sensing [5], [6]. Furthermore, this system inspired J. C. Maxwell to develop the first modern method for analyzing the stability of feedback-controlled closed-loop systems. Collectively, these examples illustrate how EI, though formally articulated only recently, has deep historical roots in mechanical design.

The formal notion of EI was first formulated in the early 1990s, primarily as a response to the limitations of symbolic *artificial intelligence* (AI). A key new idea was introduced by R. A. Brooks, who argued that intelligent behavior does not necessarily require internal representations but can in some instances arise from direct sensorimotor interaction with the environment [7]. His work on behavior-based robotics explored the notion that intelligence is grounded in physical embodiment and environmental coupling. Building upon these developments, R. Pfeifer and C. Scheier formulated a comprehensive theoretical framework that emphasizes the computational role of morphology, materials, and real-time environmental interaction in shaping behavior [8]. Specifically, regarding the main topic of this article, they state that “a fundamental consequence of embodiment is that embodied agents must interact with their environments. To understand this interaction, we have to study, for example, how organisms acquire experience: knowledge about the environment obtained by interacting with it.”

An earlier theoretical biological foundation for EI lies in the work of H. Maturana and F. Varela, who coined the concept of *autopoiesis* to describe the self-producing nature of living systems [9]. In their formulation, cognition is not simply the processing of abstract symbols or representations but is instead rooted in the dynamic and recursive interactions between an organism and its environment. This view was formalized through the idea of *structural coupling*, whereby a living system maintains its identity while continuously adapting its internal organization through sensorimotor engagement with its surroundings. Maturana and Varela claim that “*living is cognition*,” which implies that intelligent behavior emerges from the embodied self-maintaining dynamics of the organism itself. This biological perspective significantly influenced later research on embodied robotics and enactive cognitive science, fields in which intelligence is conceived as an emergent property of real-time physical interaction with the world—rather than the result of disembodied computa-

The research presented in this paper was partially funded by the Washington State University (WSU) Foundation and the Palouse Club through a Cougar Cage Award to N. O. P.-A.; the US National Science Foundation (NSF) through Award 2244082; and, the Morgan Family Charitable Trust through a direct gift to N. O. P.-A. Additional funding was provided by the WSU Voiland College of Engineering and Architecture through a start-up fund to N. O. P.-A.

The author is with the School of Mechanical and Materials Engineering, Washington State University (WSU), Pullman, WA 99164, USA. E-mail: n.perezarancibia@wsu.edu.

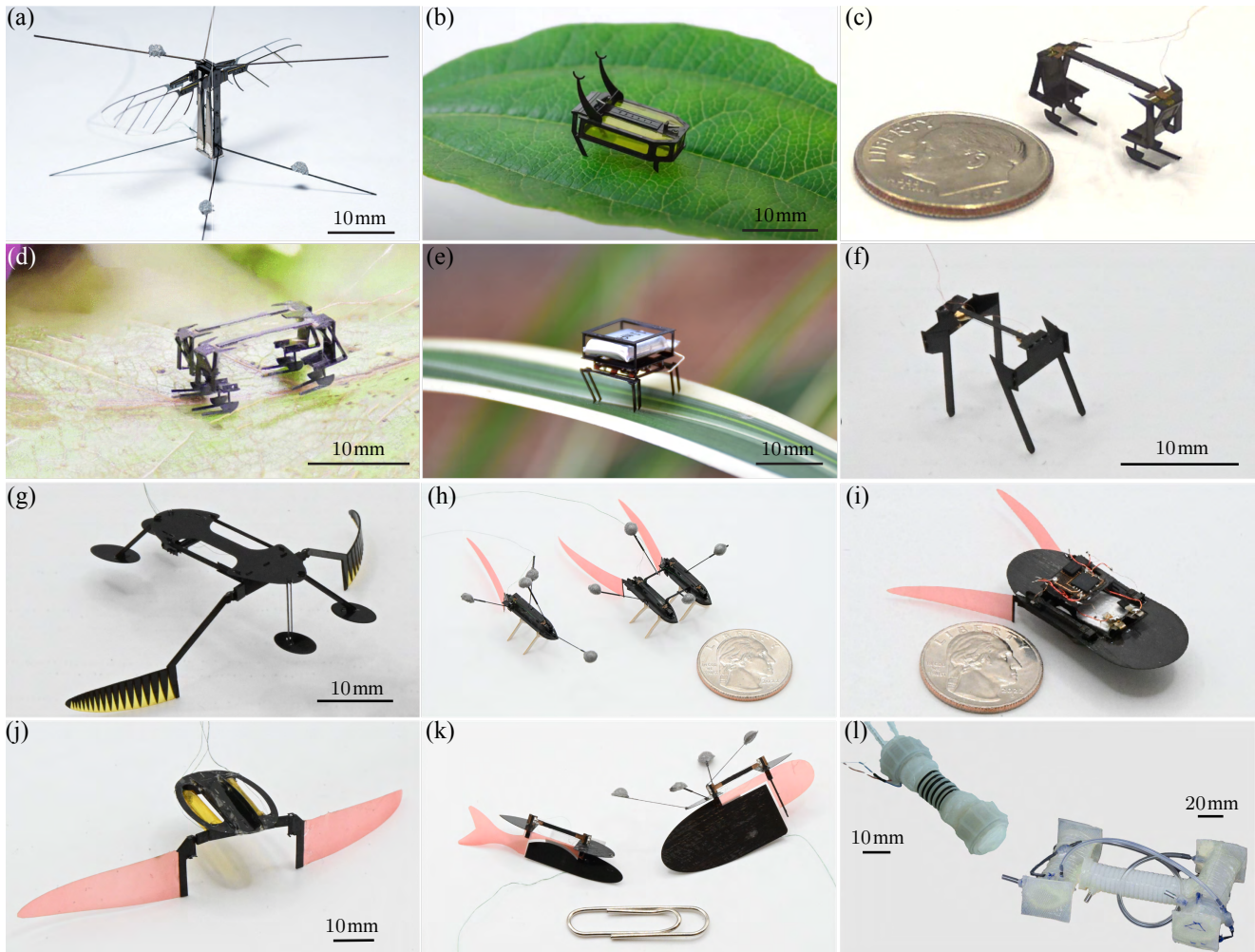


Fig. 1. Embodied intelligence in action. All the microrobots presented in this figure were developed by the author and his team at the AMSL, and each exhibits some form of EI at some level in its design. (a) The 95-mg Bee⁺⁺, which leverages FSI and an ISP-based mechanism in combination with modern nonlinear Lyapunov-based methods, to control its yaw DOF. (b) The 88-mg RoBeetle, an autonomous anisotropic-friction-based crawler mechanically powered by an NiTi–Pt composite catalytic artificial muscle. This muscle uses the flameless catalytic combustion of methanol, enabled by a rough layer of Pt, to thermally excite its core made of NiTi SMA in cycles that produce periodic actuation. The system that controls the catalytic-combustion process and the phase transitions of the SMA material is entirely electronics-free, thus leveraging EI. (c) The SMALLBug, a crawler that uses a high-frequency SMA-based bending actuator to locomote on flat surfaces. In this design, the cyclic bending motion of the driving actuator is transformed by a 2Σ-shaped frame into rectilinear locomotion through leveraging anisotropic friction. (d) The SMARTI, a crawler composed of two SMALLBug platforms connected in parallel. This configuration is 2D steerable simply by exciting its two driving actuators with phase-shifted PWM voltages, thus leveraging anisotropic friction for functionality and control. (e) The SPARQ, a fully autonomous—from both the power and control perspectives—crawler, which was conceived as an advanced version of the SMARTI. (f) The MiniBug, which, at 10 mg, is the smallest and lightest crawler with onboard actuation ever created. This robot was developed by miniaturizing the actuator and frame of the SMALLBug, and by adopting the legs of the SPARQ. (g) The WaterStrider, a surface swimmer that uses rowing-resembling motion patterns of two paddles and anisotropic drag to propel itself forward. (h) The VLEIBot (left) and VLEIBot⁺ (right) are two robots that use propulsors inspired by anguilliforms to swim forward and steer themselves. These propulsors generate thrust by leveraging FSI as traveling waves are induced by flapping soft passive fins with SMA-based bending actuators. (i) The VLEIBot⁺⁺, a fully autonomous—from both the power and control perspectives—swimmer, which was conceived as an advanced version of the VLEIBot⁺. (j) The BILLEBot, a swimmer design that combines the transmission mechanism of the WaterStrider with the traveling-wave-based thrust-generation method of the VLEIBot platform. (k) The old FRISSHBot (left) and new FRISSHBot (right) are two swimmers composed of two plates connected by an SMA-based bending actuator that applies periodic torques—with equal magnitudes and opposite directions—to both of them during operation. These actuation torques induce hydrodynamic reactive torques—generated by aggregated inertial and viscous forces—on the plates that, as a consequence, produce the thrust required for swimming. Specifically, by design, the front plate functions as an anchor and the rear plate as a caudal flapping rigid fin. This flapping fin, through the creation of a couple of vortices during an operation cycle—one clockwise and the other counterclockwise—induces a jet that, by conservation of momentum, propels the robot forward. (l) The pneumatic soft robot on the left can locomote inside pipes and trenches by leveraging pressure-controlled anisotropic friction, using a distributed stretchable artificial skin as the main sensor. The pneumatic soft robot on the right can locomote inside pipes and trenches driven by an entirely electronics-free feedback controller based on neuromorphic mechanical computation, using mechanical tactile and proprioceptive sensors.

tion or centralized control architectures.

In this paper—using as examples several robots developed by the author and his team at the *Autonomous Microrobotic Systems Laboratory* (AMSL) [10]–[22]—we contend that the basic concepts of EI, which at first sight might appear complex and abstract, can be adopted to guide the design and development of bioinspired microrobots. Through these examples, we present co-design—as opposed to modular design—as a central principle of EI, especially to address

problems relating to power, computation, and control imposed by the stringent constraints of volume and weight inherent to systems operating at the mm-to-cm-scale.

The rest of the paper is organized as follows. Section II discusses the main differences between classical control for robotics and EI in enabling complex behaviors in locomoting robots. Section III presents several examples of EI in action through the description of key features of microrobots developed by the author and his team during the past few years.

Last, Section IV summarizes the ideas presented in the paper.

II. CLASSICAL CONTROL VS. EMBODIED INTELLIGENCE

In classical control for robotics, a standard closed-loop system is composed of (i) sensors that perceive the surrounding environment and measure the state of the system; (ii) a controller that processes the information provided by the sensors, using algorithms based on mathematical laws and logic, to generate the commands that excite the system's actuators; and, (iii) the actuators that generate the forces and torques necessary to interact intelligently with the environment, according to the commands computed by the controller. This separation of perception (sensing), computation (control), and actuation requires explicit feedback, state estimation, and decision algorithms, which are predominantly implemented through the use of electronics. EI, by contrast, integrates some or all of these functions physically into the robot. For instance, morphology—including structure, compliance, and geometry—material dynamics, and control strategies can be purposely co-designed to interact with the environment so that intelligent behavior emerges through the physics of the system and its interaction with the environment.

As already hinted, here we refer to a *controller* not necessarily as an electronics-based device—analogue or digital—but, possibly, to a morphology-material-environment loop. The physical realization of this concept is clearly observable in the robots presented in [13] and [22]. From these cases, it can be inferred that the distinction between classical control and EI leads to a different robotic-design paradigm and a different set of development tools. Classical controllers are well-suited for driving highly deterministic robotic systems that operate with low levels of uncertainty—e.g., in car or semiconductor factories—where flexibility, modularity, programmability, and high precision can be achieved. Conversely, EI-based design can be employed to prioritize robustness, efficiency, and simplicity by using less general-purpose architectures. These less-general architectures, however, can be optimized for specific tasks under severe constraints. For example, EI is particularly well suited for microrobotics design because, as robots are scaled down in size and mass, conventional sources of energy and architectures become infeasible due to limitations in battery storage, computational power, and sensor integration. We believe that, at small scales, it is reasonable to design systems in which control emerges—entirely or partially—from physical design rather than exclusively from abstract computation.

Generally, to systematize EI for microrobotics development, a design framework must account for the nonlinear, often nonintuitive interactions among structure, materials, and behavior. Here, we propose a small set of heuristic EI-based design guidelines:

- i. Identify the ambient physical phenomena that can be leveraged for actuation, sensing, and control purposes—for example, anisotropic friction, anisotropic drag, buoyancy, and thermal lag.
- ii. Determine the morphological features that amplify or modulate the physical phenomena leveraged for actuation, sensing, and control.
- iii. Use analyses, numerical simulations, and experiments to understand the dynamics of the actuators that map *energy* inputs into *behavioral* outputs.
- iv. Co-design morphology and actuation to create and stabilize desired behaviors.
- v. Accept limited or more complex programmability as a tradeoff for robustness, simplicity, and weight.
- vi. Observe living systems—particularly, animals and plants—for inspiration, as intelligent behavior emerges from the embodied self-maintaining dynamics of the organisms themselves.

Next, we illustrate these ideas using some of the robots developed by the author and his team at the AMSL.

III. EMBODIED INTELLIGENCE IN ACTION

In this section, we discuss how the principles of EI—which at first sight may seem complex and ethereal—can be used to solve problems in microrobotics, in which stringent constraints relating to mass, volume, power, control, computation, sensing, and actuation must be addressed. Here, we accomplish that objective through the presentation of examples; namely, microrobots developed by the author and his team during the past six years.

A. The Bee⁺⁺: Inclined Stroke Planes for Yaw Control

The 95-mg flying Bee⁺⁺ presented in [10] and [11] is an evolved version of the Bee⁺ first presented in [12]. The latter is the first four-wing four-actuator flapping-wing insect-scale flyer ever reported, and its development was enabled by the invention of a new type of high-performance ultra-light (8.4 mg) unimorph piezoelectric actuator. A photograph of a Bee⁺⁺ prototype is shown in Fig. 1(a). The design and functionality of this prototype are depicted in Fig. 2(a). In this illustration, the vector triplets $\{n_1, n_2, n_3\}$ and $\{b_1, b_2, b_3\}$ denote the earth-fixed inertial and body-fixed frames of reference. The robot's roll *degree of freedom* (DOF) is defined as a rotation about b_1 ; accordingly, pitching and yawing are defined as rotations about b_2 and b_3 , respectively. Each of the four wings of the robot is driven by a single unimorph actuator—depicted in blue—through a four-bar mechanism of the type presented in [23]. As indicated in Figs. 2(b) and (c), the actuators are connected to their respective transmissions with an angle β , such that the stroke plane of the flapping motion is inclined relative to the b_1 - b_2 plane. The four flapping modes that enable the modulation of thrust and the roll, pitch, and yaw torques are shown in Fig. 2(d).

The motion of a Bee⁺⁺ prototype's wing can be decomposed into flapping—in direction w_3 , which coincides with b_3 —and wing-pitching—in direction w_2 , as seen in Fig. 3(a). As explained above, the flapping motion of each wing is *actively* driven by an actuator; therefore, it can be modulated and controlled as described in [10]–[12]. The pitching motion of each wing is passively generated as a flexure hinge deflects as the result of the interaction of the wing with the surrounding fluid during a flapping cycle. In this way, the thrust forces required for flight and control are produced through nonlinear *fluid-structure interaction* (FSI), a complex process very difficult to model and control explicitly. Yet, this is a clear example of morphology, actuation, and control co-design in which the ability to fly emerges as a manifestation of EI. The most notable characteristic of the Bee⁺⁺ design, however, is its ability to fly under six-DOF control using the inclined-stroke-plane-based mechanism depicted in Figs. 2(b) and (c). Specifically, this approach allowed us to robustly control the yaw DOF, a long-standing problem in bee-inspired microrobotics. As depicted in the right-bottom illustration of Fig. 2(d), by flapping the wings of the robot in diagonal pairs of identical amplitude, a pair of cyclic-averaged force components—with equal magnitudes and opposite directions—lie in the b_1 - b_2 plane at a distance from the axis b_3 , thereby generating a yaw torque that can be modulated and controlled in real time. As first presented in [12], at a frequency of 165 Hz and using Lyapunov-based nonlinear methods, sustained high-performance aerobic six-DOF-controlled flight can be achieved, as shown in Fig. 3(b). In this manner, by leveraging robotic, aerodynamic, and controller co-design—once more inspired by the notion of EI—we achieved the highest flight performance of a bee-inspired robot ever reported at the time

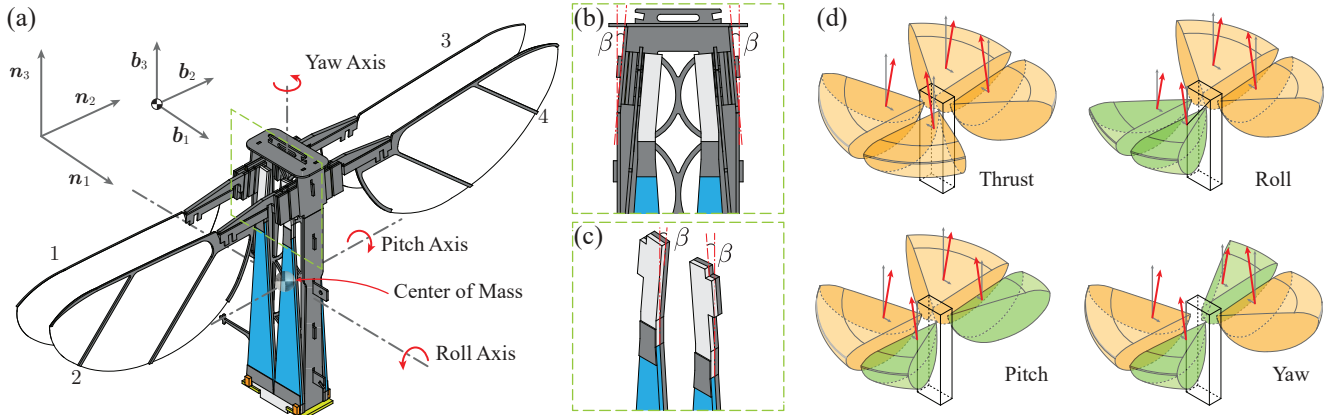


Fig. 2. The Bee⁺⁺ and its flapping modes. (a) The 95-mg Bee⁺⁺ is the first four-actuator four-wing robotic insect ever developed. As discussed in [12], this flyer is six-DOF controllable during flight. (b) Each wing is connected to its respective unimorph actuator through a four-bar transmission mechanism installed with an inclination β rad relative to the b_2 - b_3 plane—equivalent to an inclination $(\pi/2 - \beta)$ rad relative to the b_1 - b_2 plane. (c) The β -inclined installation of the robot is the result of a feature of the actuator design, whose connecting element at its distal end is tilted by the angle β . (d) The Bee⁺⁺ is underactuated as it has fewer actuators than degrees of freedom; however, it can be controlled using four basic flapping modes and nonlinear Lyapunov methods. The first mode consists of flapping the four wings of the robot with identical frequencies and amplitudes; thrust can be modulated by varying the amplitude of flapping during flight. The second mode consists of flapping the wings of the robot in pairs and asymmetrically with respect to the b_1 - b_3 plane; the roll DOF can be modulated by increasing—or decreasing—the amplitudes of flapping of one pair of wings relative to those of the other pair. The third mode consists of flapping the wings of the robot in pairs and asymmetrically with respect to the b_2 - b_3 plane; the pitch DOF can be modulated by increasing—or decreasing—the amplitudes of flapping of one pair of wings relative to those of the other pair. The fourth mode consists of flapping the wings of the robot in diagonal pairs; the yaw DOF can be modulated by increasing—or decreasing—the amplitudes of flapping of one pair of wings relative to those of the other pair. Note that the inclination of the stroke plane relative to the b_1 - b_2 plane generates a yaw torque that can be modulated to actuate and control the yaw DOF, thus exemplifying EI in action.

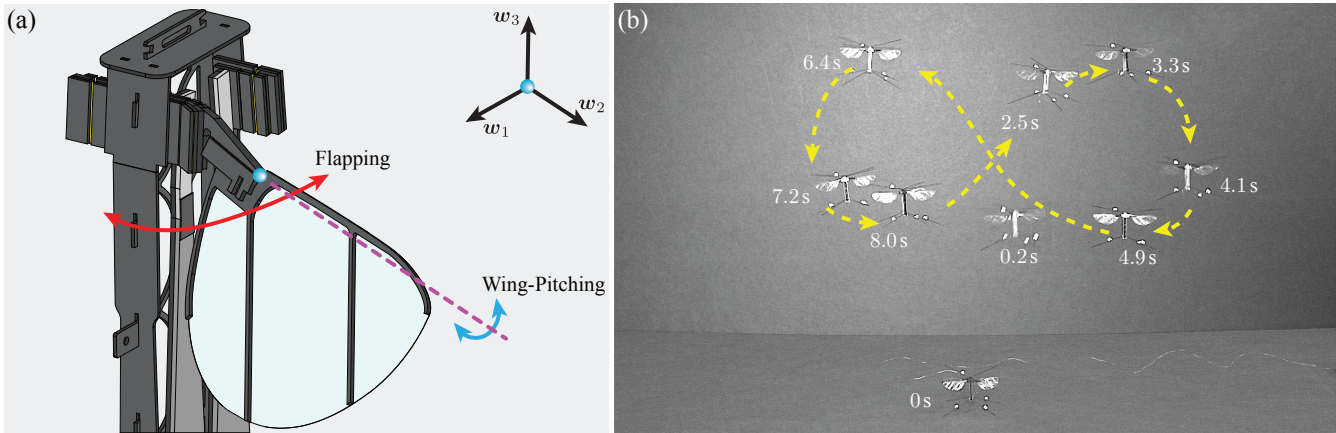


Fig. 3. Wing motion during flight and aerobatic maneuver. (a) Active flapping and passive wing-pitching. The flapping motion is generated through a four-bar mechanism transmission by a unimorph actuator; in contrast, the wing-pitching motion is the result of FSI. Combined with the inclined-stroke-plane-based mechanism for yaw control, the passive pitching of the wing exemplifies a case of EI in action. (b) A Bee⁺⁺ prototype during aerobatic flight. In this case, the yaw DOF was controlled by combining the ISP-based mechanism with nonlinear Lyapunov-based control schemes. This case demonstrates that EI and modern control are not incompatible and can be employed in conjunction.

of publication. Video footage of a flight test of this type is shown in the accompanying supplementary movie.

B. The RoBeetle: A Crawler Driven by an Artificial Muscle Controlled Using an Electronics-Free Mechanism

The RoBeetle shown in Fig. 1(b)—first presented in [13]—is an 88-mg autonomous crawler that leverages anisotropic friction to locomote and is actuated by a catalytic artificial muscle. The functionality of this actuator is depicted in Fig. 4. The muscle has a thin cylindrical core (a wire) made of *shape-memory alloy* (SMA) nitinol and a rough granular layer made of platinum (Pt) particles. An SMA wire under tension can be thermally excited according to homogeneous cycles of heating and cooling to generate periodic actuation, as the wire cyclically contracts and extends. This phenomenon is graphically explained in Fig. 4(a), which depicts an actuation cycle that starts with the SMA wire extended because its SMA material is in a *detwinned martensite* state

at room temperature (20°C). Then, through the application of heat, the SMA material transitions to *austenite* and, as a consequence, the wire contracts. When the material is left to cool down by free convection, it transitions to a *twinned martensite* state. Last in an actuation cycle, the application of stress detwines the SMA material, and the wire returns to its initial condition. In the case of the muscle actuating the RoBeetle, heat is applied cyclically using catalytic combustion, as shown in Fig. 4(b). This method leverages the catalytic capability of Pt, which facilitates the flameless combustion of a wide variety of fuels, including hydrogen, propane, butane, and methanol. Given that the nominal transition temperature of the SMA wire (Dynalloy NiTi with a diameter of 50.8 μm) driving the RoBeetle is 90°C, we selected methanol as the source of energy because it ignites catalytically—using Pt as the catalyst—at temperatures as low as 40°C and can be stored easily in liquid form. Furthermore, the specific energy of methanol is

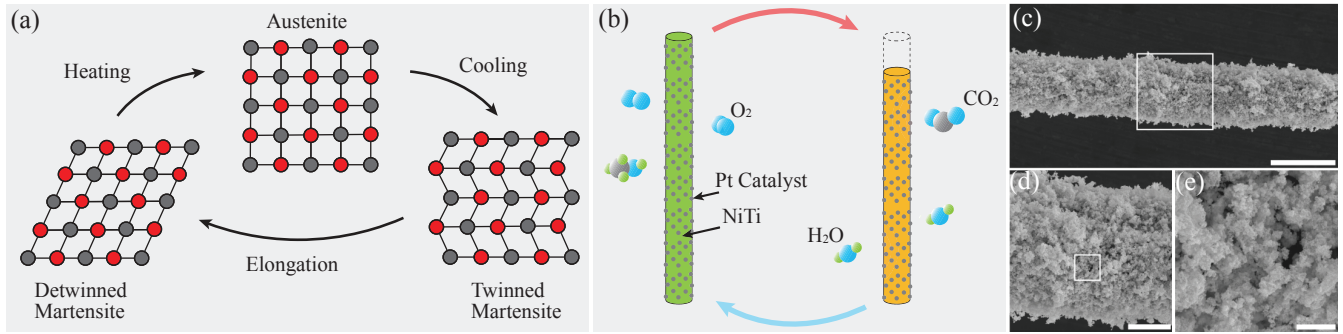


Fig. 4. Functionality of the catalytic artificial muscle developed to drive the RoBeetle shown in Fig. 1(b). (a) During a full actuation cycle, the material of an SMA wire transitions between three distinct crystal-structure states: *detwinned martensite*, *austenite*, and *twinned martensite* by the sequential application of heat, allowance for convective cooling, and application of stress. (b) In the case of the RoBeetle’s muscle, controlled heat is applied through the catalytic combustion of methanol—facilitated by a rough layer of Pt, a multipurpose catalyst—and stress is applied using a CF leaf spring (shown in Fig. 5(b)). Accordingly, an actuation cycle starts at the detwinned martensite state—corresponding to the extended state of the wire at room temperature; then, after surpassing the transition temperature of the SMA material, the system transitions to the austenite state—corresponding to the contracted state of the wire; next, after cooling down through free convection and reaching room temperature, the system transitions to the martensite state. The stress applied by the leaf spring to the wire continually detwines the SMA material. (c)–(e) SEM images of the surface of a NiTi-Pt composite wire with a diameter of 87 μm . The rough and porous catalytic layer (Pt-black) has a thickness of 18.1 μm . The magnifications of the images are $\times 350$, $\times 1200$, and $\times 6500$; the scale bars indicate distances of 100, 30, and 5 μm , respectively.

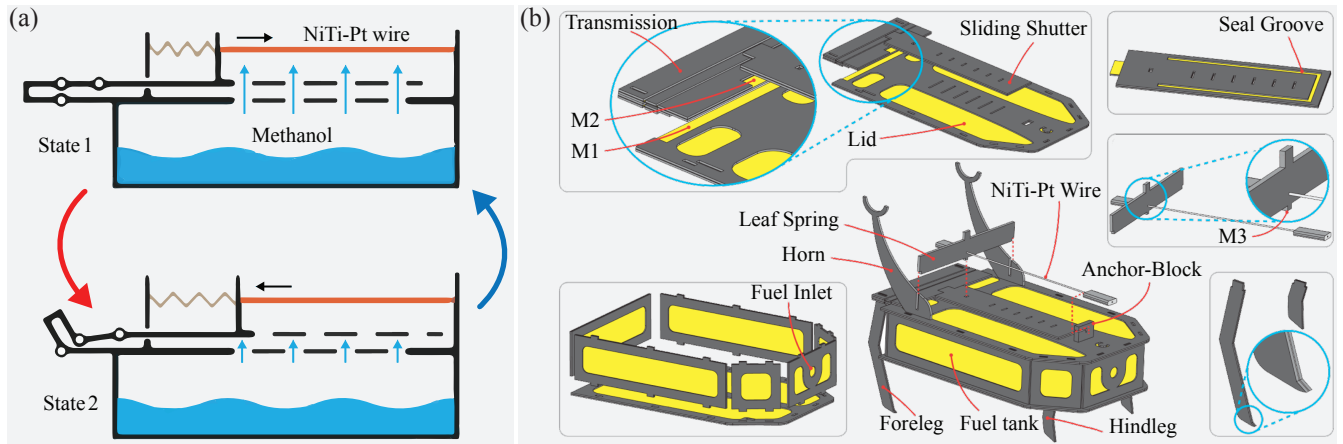


Fig. 5. Design and functionality of the RoBeetle platform. (a) Mechanical system that controls the catalytic-combustion process and the phase transitions of the muscle’s SMA material without electronics, thereby leveraging EI; the robot’s body simultaneously functions as an actuator, a sensor, and a mechanical controller. (b) The RoBeetle and its functional components. In this illustration, the labels M1, M2, and M3 denote mating points of assembly fixtures.

on the order of 20 MJ/kg, which is substantially higher than that of the best state-of-the-art Lithium-ion (Li-ion) batteries available today, which ranges from 0.9 to 1.3 MJ/kg.

Three images obtained using *scanning electron microscopy* (SEM)—with three levels of magnification—are presented in Figs. 4(c)–(e). We discovered experimentally that a highly granular and rough structure of this type is required to initiate and sustain catalytic combustion for actuation. In principle, the idea of using a catalytic muscle of the type shown in Fig. 4(b) to mechanically power a subgram mm-scale crawler is straightforward. However, to implement this idea, we need to control two complex systems simultaneously under extremely stringent constraints of power, volume, and mass. These constraints greatly limit the possibility of using sophisticated sensing, electronics, and computation according to the classical control for robotics paradigm discussed in Section II. To solve this problem, we designed a system that controls the catalytic-combustion process and the phase transitions of the muscle’s SMA material without electronics, thereby leveraging EI; the robot’s body simultaneously functions as an actuator, a sensor, and a mechanical controller, as depicted in Figs. 5(a) and (b). In summary, the RoBeetle’s design embodies intelligence by controlling gait dynamics using structural stiffness and unactuated valving, enabling

forward locomotion without any electronic feedback. Gait control emerges from the interplay of structural elasticity, actuator timing, and surface-contact friction. The electrically powered SMALLBug platform shown in Fig. 1(c) employs a similar mode of locomotion, as shown in Fig. 6(a). A photographic composite of a RoBeetle prototype crawling on a flat surface is shown in Fig. 7(a). Video footage of an experiment of this type is shown in the accompanying supplementary movie.

C. SMA-Based Bending Actuation and Anisotropic Friction for Locomotion on Flat Surfaces

The SMALLBug—the crawler shown in Fig. 1(c)—uses a high-frequency SMA-based bending actuator of the type shown on the left in Fig. 6(a) to locomote on flat surfaces. In this design, the two SMA wires of the actuator are connected under tension in parallel to a *carbon fiber* (CF) beam, as described in [14]. Accordingly, when the SMA material of the wires is cyclically Joule heated and cooled down by free convection—as explained in Section III-B and depicted in Fig. 4(a)—periodic actuation is produced as the SMA wires sequentially transition under tension from the detwinned martensite state to the austenite state, then to the twinned martensite state, and, last in the cycle, back to the detwinned

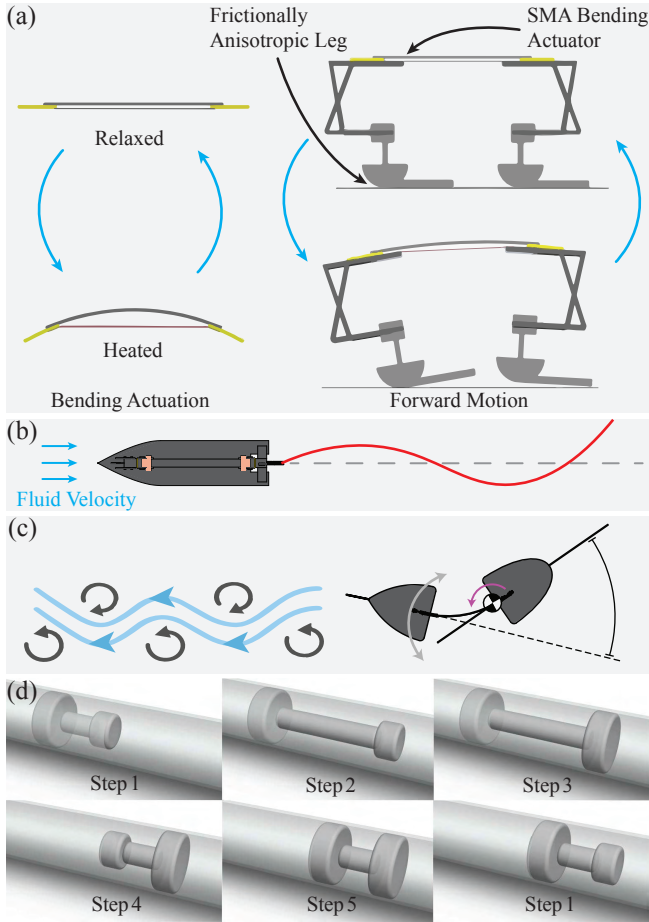


Fig. 6. Mechanisms of locomotion, leveraging EI, of some of the robots discussed in this article. (a) Bending actuator (left) and anisotropic-friction-based locomotion mode of the SMALLBug platform shown in Fig. 1(c). (b) Swimming thrust generated by a traveling wave passing through the unactuated soft slender tail of a VLEIBot prototype shown in Fig. 1(h). (c) Swimming thrust generated by tail-generated vortices used by the FRISSHBot platforms, shown in Fig. 1(k), to propel themselves forward. (d) Basic locomotion mechanism used by the pneumatic soft robots shown in Fig. 1(l).

martensite state. In this idealization, the CF beam functions as a leaf spring that facilitates the detwinning process of the SMA material. As shown on the right in Fig. 6(a), the cyclic bending motion of the driving actuator is transformed by a 2Σ -shaped frame into rectilinear locomotion by leveraging anisotropic friction.

The SMALLBug design materializes the notion of EI because the mechanical, thermodynamic, and material properties of the driving SMA-based actuator—and its integration with the robot’s frame and legs—enable locomotion patterns to emerge without explicit sensing, computation, or complex control logic. For example, when its actuator is excited using a *pulse-width modulation* (PWM) voltage, changing actuation frequency alone switches gaits between crawling (2 Hz), shuffling (10 Hz), and galloping (20 Hz). Notably, different locomotion modes emerge from actuator–body–environment interaction, without the need for active gait control. The SMARTI—the crawler shown in Fig. 1(d)—is composed of two SMALLBug platforms connected in parallel. This configuration is 2D steerable by simply exciting its two driving actuators with phase-shifted PWM voltages; thereby once more leveraging anisotropic friction for functionality and control. Pushing the EI-enabled approach further, we developed the SPARQ, shown in Fig. 1(e), and MiniBug, shown

in Fig. 1(f). The SPARQ at 500 mg (including its battery) is the lightest autonomous crawler developed to date, and the MiniBug at 10 mg is the lightest and smallest crawler with onboard actuation ever reported. A photographic composite of a MiniBug prototype crawling on a flat surface is shown in Fig. 7(b). Video footage of six experiments of this type is shown in the accompanying supplementary movie.

D. Anisotropic Drag for Surface Swimming

The WaterStrider—shown in Fig. 1(g)—is a surface swimmer bioinspired by *Gerridae* [16]. Similarly to the crawlers discussed in Section III-C, this robot is driven by two SMA-based bending actuators and leverages EI-inspired methods to function. Specifically, it propels itself forward using anisotropic drag and floats by means of the surface tension of water. Using a rowing-resembling submicircular motion pattern, its two swimming appendages rotate rigidly (generating relatively high drag) during the power stroke and compliantly during the reverse stroke (generating relatively low drag). Thus, once more, locomotion emerges from the integration of morphology and materials, and environmental interactions, rather than from complex computation or sensing. In this sense, the WaterStrider *embodies* intelligence, as it achieves functional behaviors—floating, moving, turning—through design choices that leverage the interaction with the environment, thus offloading computational burden to morphology and material properties. Photographic composites of a WaterStrider prototype swimming excited by four different open-loop signals are shown in Fig. 7(c). Footage of a test of this type is shown in the supplementary movie.

E. FSI-Based Generation of Traveling Waves for Swimming

The VLEIBot, VLEIBot⁺, VLEIBot⁺⁺, and BILLEBot platforms, first presented in [17]–[19], are shown in Figs. 1(h)–(j). As seen, the first robot is propelled by a single propulsor and the last three robots by two. Each propulsor is composed of two main elements: (i) an SMA-based bending actuator of the type discussed in Section III-C; and, (ii) a passive flexible hydrofoil, which functions as a propulsive fin. As depicted in Fig. 6(b), when a propulsive fin of the type driving the robots shown in Figs. 1(h)–(j) is flapped by its actuator, a traveling wave is generated through a complex nonlinear mechanism of FSI. Fully understanding how a traveling wave is created through FSI is an extremely difficult task and requires the use of *computational fluid dynamics* (CFD). However, using the methods discussed in [24]–[26] and video analyses, we can estimate the generated propulsive forces by considering the fin’s motion to be fully prescribed and produced by a *virtual actuator*. This approach is based on the notion of *added mass*, assuming a slender body of the propulsive tail; therefore, it accounts for the reactive (inertial) hydrodynamic forces acting on the swimmer’s body, while resistive (viscous) forces are entirely neglected. Despite these limitations, we have consistently used this method for robotic and controller design. The robots discussed in this subsection exemplify EI because their propulsion arises from the physical coupling of SMA-based actuators, flexible fins, and surrounding fluid. Through FSI, traveling waves and, as a result, propulsive forces emerge naturally without requiring complex computation or control. Thus, functionality and efficiency are achieved by exploiting morphology and physical phenomena directly, rather than relying solely on control algorithms. Photographic composites of a BILLEBot prototype swimming excited by two different open-loop signals are shown in Fig. 7(d). Video footage of a test of this type is shown in the accompanying supplementary movie.

F. Swimming by Tail-Generated Vortices

Fig. 1(k) shows the old (left) and new (right) FRISSHBot platforms [20], [21]. These two swimmers are composed of

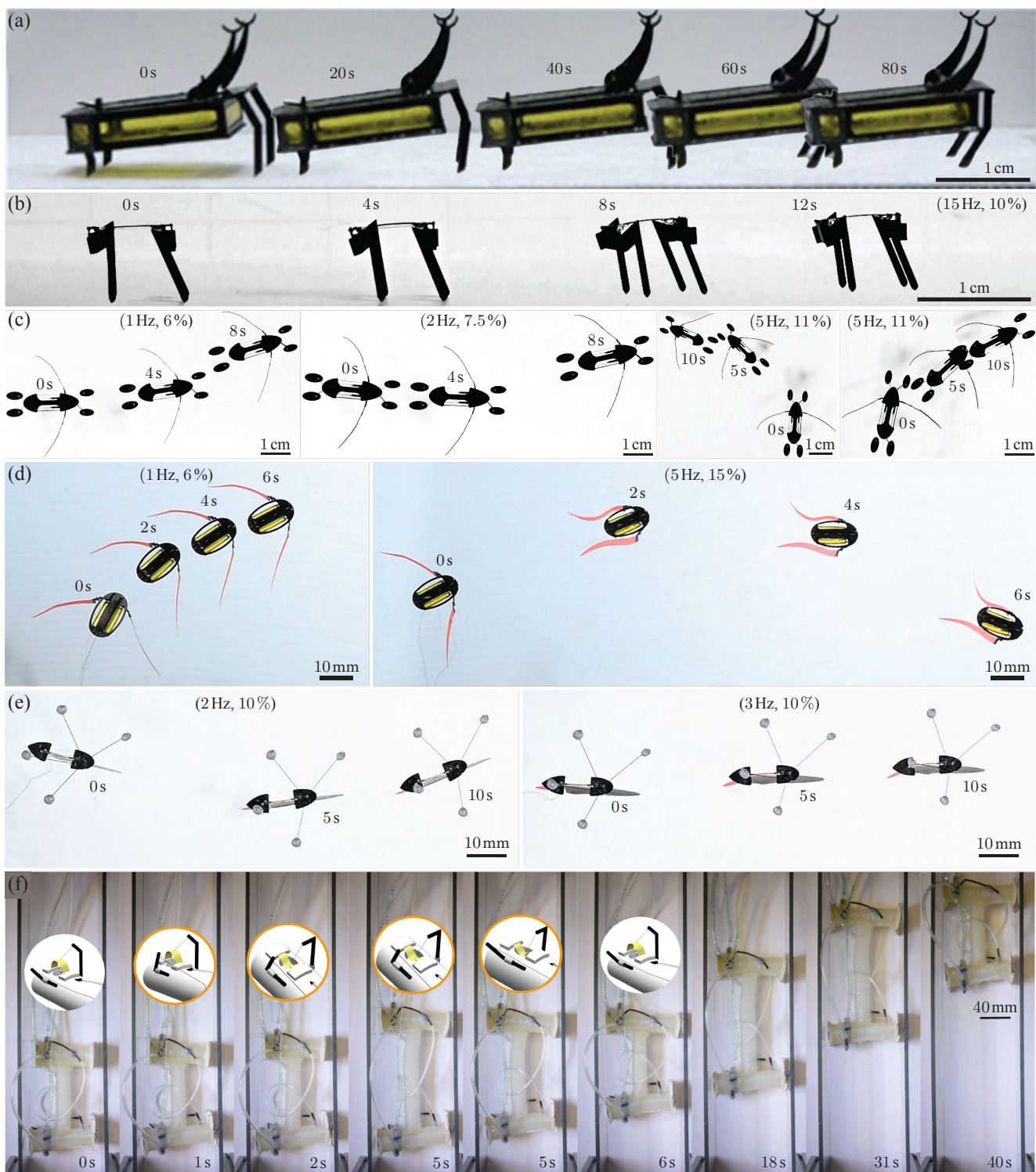


Fig. 7. Photographic composites of images showing locomotion tests of six of the robots discussed in this article. (a) A RoBeetle prototype crawling on a flat surface. (b) A MiniBug prototype crawling on a flat surface, excited with a 15-Hz PWM signal with a DC of 10%. (c) A WaterStrider prototype swimming excited by four different PWM signals with the frequencies and DC values in parentheses. (d) A BILLEBot prototype swimming excited by two different PWM signals with the frequencies and DC values in parentheses. (e) A FRISSHBot prototype swimming excited by two different PWM signals with the frequencies and DC values in parentheses. (f) Electronics-free pneumatic-based soft robot, shown on the right in Fig. 1(l), crawling inside a trench. This robot is feedback-controlled using neuromorphic mechanical computation and mechanical tactile and proprioceptive sensors.

two plates connected by an SMA-based bending actuator that applies periodic torques—with identical magnitudes and opposite directions—to both plates during operation. The actuation torques induce hydrodynamic reactive torques—

generated by aggregated inertial and viscous forces—on the two plates which, as a consequence, produce the thrust required for swimming. Specifically, by design, the front plate functions as an anchor and the rear plate as a caudal

fin. A caudal fin generates thrust by flapping laterally in a way that sheds a series of coherent vortices into the surrounding fluid. These resulting vortices, as a whole, can be thought of as a reverse von Kármán vortex street, which produces a narrow, high-speed jet directed rearward. By conservation of momentum, the rearward jet induces a forward reactive force on the robot's body, as shown in Fig. 6(c). The efficiency of this mechanism is closely tied to the Strouhal number, which quantifies the relative importance of vortex spacing, tail-beat frequency, and swimming speed. In [27], it is argued that vortex-based jet formation is the fundamental fluid-dynamic process by which caudal fins propel swimming machines—including fish—efficiently. The FRISSHBot platforms embody intelligence by exploiting hydrodynamic laws through their morphology and interaction with the surrounding fluid. The oscillations of their fins shed vortices and form thrust-generating jets, thereby reducing control complexity. Photographic composites of a FRISSH-Bot prototype swimming excited by two different open-loop signals are shown in Fig. 7(e). Video footage of a test of this type is shown in the accompanying supplementary movie.

G. Earthworm-Inspired Locomotion, Perceptive Skins, and Neuromorphic Mechanical Computation

The pneumatic soft robot on the left in Fig. 1(l) can locomote inside pipes and trenches by leveraging pressure-controlled anisotropic friction according to the pattern shown in Fig. 6(d), using as sensors a distributed stretchable artificial skin [28]. The pneumatic soft robot on the right in Fig. 1(l) can locomote inside pipes and trenches driven by an entirely electronics-free feedback controller based on neuromorphic mechanical computation, conceptualized according to the notions in [29], using electronics-free tactile and proprioceptive sensors [22]. These designs exemplify EI by integrating sensing, actuation, and control directly into the robot's body. The use of pressure-controlled anisotropic friction and stretchable skins allows locomotion and perception to emerge from material properties rather than from electronics, control, and computation. Likewise, inspired by EI, the neuromorphic mechanical controller achieves feedback regulation by leveraging the intrinsic mechanical dynamics of the robot instead of using electronics. Together, these features demonstrate how morphology and distributed sensing can enable autonomous functionality through embodiment. This feature is especially important in soft robotics. A photographic sequence of the soft robot on the right in Fig. 1(l) locomoting inside a trench is shown in Fig. 7(f). Video footage of a test of this type is presented in the accompanying supplementary movie.

IV. CONCLUSION

EI, rooted in physical co-design, challenges the traditional view that intelligence resides solely in centralized—digital or analog—computation. Electronics-free microrobots illustrate how control, sensing, and actuation can emerge from morphology and material response. In contrast to classical robotic systems with isolated modules, EI requires integration. As microrobotics advances toward autonomy under extreme constraints, embodied approaches offer both a theoretical foundation and a practical path forward. Embodied systems are not just artifacts of constrained robotics—they are demonstrations of a deeper principle: that behavior can be designed into matter itself. Co-design is not just a method, but an intellectual approach to research and development.

REFERENCES

- [1] A. G. Drachmann, *Ktesibios, Philon, and Heron: A Study in Ancient Pneumatics*. Copenhagen, Denmark: Munksgaard, 1948.
- [2] B. Woodcroft, *Pneumatics of Hero of Alexandria*. London, UK: Taylor Walton and Maberly, 1851.
- [3] D. R. Hill, *The Book of Knowledge of Ingenious Mechanical Devices*. Dordrecht, Netherlands: Springer, 1974, Translated from the Original Arabic Manuscript by Al-Jazari.
- [4] J. Essinger, *Jacquard's Web: How a Hand-Loom Led to the Birth of the Information Age*. Oxford, UK: Oxford University Press, 2004.
- [5] J. C. Maxwell, "On Governors," *Proc. Roy. Soc. Lond.*, vol. 16, pp. 270–283, Jan. 1867.
- [6] S. Bennett, *A History of Control Engineering, 1800–1930*. London, UK: Institution of Electrical Engineers (IET), 1979.
- [7] R. A. Brooks, "Intelligence Without Representation," *Artif. Intell.*, vol. 47, no. 1–3, pp. 139–159, 1991.
- [8] R. Pfeifer and C. Scheier, *Understanding Intelligence*. Cambridge, MA, USA: MIT Press, 1999.
- [9] H. R. Maturana and F. J. Varela, *Autopoiesis and Cognition: The Realization of the Living*. Dordrecht, Netherlands: D. Reidel Publishing Company, 1980.
- [10] X. Yang, Y. Chen, L. Chang, A. A. Calderón, and N. O. Pérez-Arancibia, "Bee⁺: A 95-mg Four-Winged Insect-Scale Flying Robot Driven by Twinned Unimorph Actuators," *IEEE Robot. Autom. Lett.*, vol. 4, pp. 4270–4277, Jul. 2019.
- [11] R. M. Bena, X.-T. Nguyen, X. Yang, A. A. Calderón, Y. Chen, and N. O. Pérez-Arancibia, "A Multiplatform Position Control Scheme for Flying Robotic Insects," *J. Intell. Robot. Syst.*, vol. 105, May 2022, Art. no. 19.
- [12] R. M. Bena, X. Yang, A. A. Calderón, and N. O. Pérez-Arancibia, "High-Performance Six-DOF Flight Control of the Bee⁺: An Inclined-Stroke-Plane Approach," *IEEE Trans. Robot.*, vol. 39, pp. 1668–1684, Apr. 2023.
- [13] X. Yang, L. Chang, and N. O. Pérez-Arancibia, "An 88-Milligram Insect-Scale Autonomous Crawling Robot Driven by a Catalytic Artificial Muscle," *Sci. Robot.*, vol. 5, Aug. 2020, Art. no. eaba0015.
- [14] X.-T. Nguyen, A. A. Calderón, A. Rigo, J. Z. Ge, and N. O. Pérez-Arancibia, "SMALLBug: A 30-mg Crawling Robot Driven by a High-Frequency Flexible SMA Microactuator," *IEEE Robot. Autom. Lett.*, vol. 5, no. 4, pp. 6796–6803, Oct. 2020.
- [15] R. M. Bena, X.-T. Nguyen, A. A. Calderón, A. Rigo, and N. O. Pérez-Arancibia, "SMART: A 60-mg Steerable Robot Driven by High-Frequency Shape-Memory Alloy Actuation," *IEEE Robot. Autom. Lett.*, vol. 6, no. 4, pp. 8173–8180, Oct. 2021.
- [16] C. K. Trygstad, X.-T. Nguyen, and N. O. Pérez-Arancibia, "A New 1-mg Fast Unimorph SMA-Based Actuator for Microrobotics," in *Proc. IEEE/RSJ Int. Conf. Intell. Robots Syst. (IROS)*, Detroit, MI, USA, Oct. 2023, pp. 2693–2700.
- [17] E. K. Blankenship, C. K. Trygstad, F. M. F. R. Gonçalves, and N. O. Pérez-Arancibia, "VLEIBot: A New 45-mg Swimming Microrobot Driven by a Bioinspired Anguilliform Propulsor," in *Proc. IEEE Int. Conf. Robot. Autom. (ICRA)*, Yokohama, Japan, May 2024, pp. 6014–6021.
- [18] C. R. Longwell, C. K. Trygstad, and N. O. Pérez-Arancibia, "Power-Efficient Actuation for Insect-Scale Autonomous Underwater Vehicles," in *Proc. Int. Symp. Robot. Res. (ISRR)*, Long Beach, CA, USA, Dec. 2024, Art. no. 39.
- [19] C. K. Trygstad, C. R. Longwell, F. M. F. R. Gonçalves, and N. O. Pérez-Arancibia, "A 93-Milligram Submersible Swimmer Driven by Energy-Efficient SMA-Based Millimeter-Scale Actuators," *npj Robotics*, 2025, to appear.
- [20] C. K. Trygstad, E. K. Blankenship, and N. O. Pérez-Arancibia, "A New 10-mg SMA-Based Fast Bimorph Actuator for Microrobotics," in *Proc. IEEE/RSJ Int. Conf. Intell. Robots Syst. (IROS)*, Abu Dhabi, UAE, Oct. 2024, pp. 1349–1356.
- [21] C. K. Trygstad, C. R. Longwell, F. M. F. R. Gonçalves, E. K. Blankenship, and N. O. Pérez-Arancibia, "Feedback Control of a Single-Tail Bioinspired 59-mg Swimmer," in *Proc. IEEE/RSJ Int. Conf. Intell. Robots Syst. (IROS)*, Hangzhou, China, Oct. 2025, pp. 5722–5729.
- [22] K. Xu and N. O. Pérez-Arancibia, "Electronics-Free Logic Circuits for Localized Feedback Control of Multi-Actuator Soft Robots," *IEEE Robot. Autom. Lett.*, vol. 5, no. 3, pp. 3990–3997, Jul. 2020.
- [23] R. J. Wood, "The First Takeoff of a Biologically Inspired At-Scale Insect Robot," *IEEE Trans. Robot.*, vol. 24, no. 2, pp. 341–347, Apr. 2008.
- [24] M. J. Lighthill, "Note on the Swimming of Slender Fish," *J. Fluid Mech.*, vol. 9, no. 2, pp. 305–317, Oct. 1960.
- [25] —, "Large-Amplitude Elongated-Body Theory of Fish Locomotion," *Proc. R. Soc. Lond. B Biol. Sci.*, vol. 179, no. 1055, pp. 125–138, Nov. 1971.
- [26] T. Y.-T. Wu, "Hydromechanics of Swimming Propulsion. Part 1. Swimming of a Two-Dimensional Flexible Plate at Variable Forward Speeds in an Inviscid Fluid," *J. Fluid Mech.*, vol. 46, no. 2, pp. 337–355, Mar. 1971.
- [27] M. S. Triantafyllou and G. S. Triantafyllou, "An Efficient Swimming Machine," *Sci. Am.*, vol. 272, no. 3, pp. 64–70, Mar. 1995.
- [28] A. A. Calderón, J. C. Ugalde, L. Chang, J. C. Zagal, and N. O. Pérez-Arancibia, "An earthworm-inspired soft robot with perceptive artificial skin," *Bioinspir. Biomim.*, vol. 14, no. 5, Sep. 2019, Art. no. 056012.
- [29] W. S. McCulloch and W. H. Pitts, "A Logical Calculus of the Ideas Immanent in Nervous Activity," *Bull. Math. Biophys.*, vol. 5, no. 4, pp. 115–133, Dec. 1943.